

# Ultraviolet Raman Examination of the Environmental Dependence of Bombolitin I and Bombolitin III Secondary Structure

Janet S. W. Holtz, John H. Holtz, Zhenhuan Chi, and Sanford A. Asher

Department of Chemistry, University of Pittsburgh, Pittsburgh, Pennsylvania 15260 USA

**ABSTRACT** Bombolitin I and III (BI and BIII) are small amphiphilic peptides isolated from bumblebee venom. Although they exist in predominately nonhelical conformations in dilute aqueous solutions, we demonstrate, using UV Raman spectroscopy, that they become predominately  $\alpha$ -helical in solution at pH > 10, in high ionic strength solutions, and in the presence of trifluoroethanol (TFE) and dodecylphosphocholine (DPC) micelles. In this paper, we examine the effects of electrostatic and hydrophobic interactions that control folding of BI and BIII by systematically monitoring their secondary structures as a function of solution conditions. We determine the BI and BIII secondary structure contents by using the quantitative UV Raman methodology of Chi et al. (1998, *Biochemistry*, 37:2854–2864). Our findings suggest that the  $\alpha$ -helix turn in BIII at neutral pH is stabilized by a salt bridge between residues Asp<sup>2</sup> and Lys<sup>5</sup>. This initial  $\alpha$ -helical turn results in different BI and BIII  $\alpha$ -helical folding mechanisms observed in high pH and high salt concentrations: BIII folds from its single  $\alpha$ -helix turn close to its N-terminal, whereas the BI  $\alpha$ -helix probably nucleates within the C-terminal half. We also used quasielastic light scattering to demonstrate that the BI and BIII  $\alpha$ -helix formation in 0.2 M Ca(ClO<sub>4</sub>)<sub>2</sub> is accompanied by formation of trimers and hexamers, respectively.

## INTRODUCTION

A balance of electrostatic and hydrophobic interactions, along with structural constraints, determines peptide and protein conformations. An elucidation of these factors is critical for understanding protein folding mechanisms. The effects of electrostatic and hydrophobic interactions on peptide/protein structure can be studied by examining the dependence of peptide and protein structure on different solution environments. For example, electrostatic interactions can be studied by perturbing their interactions by changing the pH or adding ions. For example, Goto et al. (1990) have shown that acid-denatured cyc *c* and apoMb at low ionic strengths refold with the addition of ions. Perturbation of hydrophobic interactions can be accomplished by using sodium dodecylsulfate (SDS) (Waterhous and Johnson, 1994; Chupin et al., 1995) and dodecylphosphocholine (DPC) (Chupin et al., 1995; Javadpour and Barkley, 1997) micelles to provide a heterogeneous amphiphilic environment. Hydrophobic effects in peptides/proteins can also be perturbed by adding trifluoroethanol (TFE), which is sometimes used to mimic the homogeneous hydrophobic interactions of membranes (Chupin et al., 1995; Albert and Hamilton, 1995).

We selected bombolitin I (BI) and bombolitin III (BIII), two structurally similar heptadecapeptides isolated from bumblebee venom (Argiolas and Pisano, 1985), to study the environmental dependence of protein structure, because they change from predominately nonhelical in dilute solution to predominately  $\alpha$ -helical at high peptide concentra-

tions (Bairaktari et al., 1990a), at high ionic strength, at high pH (Bairaktari et al., 1990a), and upon exposure to micelles/bilayers and TFE.

The primary sequences of BI and BIII only differ at positions 4, 5, and 6:

BI: Ile<sup>1</sup>-Lys<sup>2</sup>-Ile<sup>3</sup>-Thr<sup>4</sup>-Thr<sup>5</sup>-Met<sup>6</sup>-Leu<sup>7</sup>-Ala<sup>8</sup>-Lys<sup>9</sup>-Leu<sup>10</sup>-Gly<sup>11</sup>-Lys<sup>12</sup>-Val<sup>13</sup>-Leu<sup>14</sup>-Ala<sup>15</sup>-His<sup>16</sup>-Val<sup>17</sup>-NH<sub>2</sub>

BIII: Ile<sup>1</sup>-Lys<sup>2</sup>-Ile<sup>3</sup>-Met<sup>4</sup>-Asp<sup>5</sup>-Ile<sup>6</sup>-Leu<sup>7</sup>-Ala<sup>8</sup>-Lys<sup>9</sup>-Leu<sup>10</sup>-Gly<sup>11</sup>-Lys<sup>12</sup>-Val<sup>13</sup>-Leu<sup>14</sup>-Ala<sup>15</sup>-His<sup>16</sup>-Val<sup>17</sup>-NH<sub>2</sub>

Yet, they show significantly different secondary structural dependences on environment.

In this study, we used UV resonance Raman spectroscopy (UVRR) to quantify the BI and BIII secondary structures under various solution conditions. We utilized the methodology developed by Chi et al. (1998), which simultaneously uses the Raman amide I, II, III bands and the C <sub>$\alpha$</sub> -H bending bands to determine protein secondary structure.

BI and BIII are ideal candidates for 206.5-nm UVRR secondary structure investigations, because they contain no aromatic amino acids, whose resonance Raman spectra overlap the amide vibrational bands. 206.5-nm excitation occurs within the amide  $\pi$ - $\pi^*$  transitions (Song and Asher, 1989), which selectively enhances the amide I, II, III, and the C <sub>$\alpha$</sub> -H bending bands. Thus we can easily quantify the BI and BIII secondary structures as a function of solution conditions.

## MATERIALS AND METHODS

BI and BIII were synthesized and purified by the peptide facility at the Pittsburgh Cancer Institute of the University of Pittsburgh (Pittsburgh, PA). Ammonium hydroxide and hydrochloric acid were purchased from Mallinckrodt (Paris, KY). Sodium chloride and calcium chloride dihydrate were purchased from EM Science (Cherry Hill, NJ). Sodium perchlorate, calcium perchlorate tetrahydrate, and trifluoroethanol (ol-d) (TFE) were pur-

Received for publication 29 April 1998 and in final form 1 March 1999.

Address reprint requests to Dr. Sanford A. Asher, Department of Chemistry, University of Pittsburgh, Pittsburgh, PA 15260. Tel.: 412-624-8570; Fax: 412-624-0588; E-mail: asher+@pitt.edu.

© 1999 by the Biophysical Society

0006-3495/99/06/3227/08 \$2.00

chased from Aldrich Chemicals (Milwaukee, WI). Dodecylphosphocholine (DPC) was obtained from Avanti Polar Lipids (Alabaster, AL).

### Quasielastic light scattering experiments

Quasielastic light scattering (QELS) measurements were made with a miniDAWN (Wyatt Technology) QELS instrument with a multiangle light scattering detector and a 30-mW, 690-nm solid-state laser. Measurements were made in the dynamic mode, where  $\sim 0.5$  ml of 0.22 mM peptide solutions flowed through a 0.1- $\mu\text{m}$  syringe filter as they were injected at the rate of 0.2 ml/min. The signal from the detector was collected and analyzed with Astra software.

### UV resonance Raman spectroscopy

We utilized 206.5-nm excitation from an intracavity frequency-doubled CW krypton ion laser (Holtz et al., 1996) to excite within the amide  $\pi-\pi^*$  transitions, to selectively enhance the amide vibrations. Approximately 0.6 mW laser power was focused onto the sample. The Raman scattered light was collected in a  $135^\circ$  back-scattering geometry from a spinning quartz cell containing 0.5 ml of a 0.22 mM peptide solution and dispersed by a Spex TripleMate spectrograph (Asher et al., 1983; Asher, 1993a,b). The spectra were detected with an intensified CCD detector (model ICCD-1024 MS-E; Princeton Instruments). The total accumulation time for each spectrum was 5 min. We utilized a  $\sim 20\text{-cm}^{-1}$  spectral resolution.

The secondary structures of BI and BIII in various solution environments were determined by a methodology developed by Chi et al. (1998), which calculates the protein secondary structure fractional abundance by least-squares fit of the protein Raman spectrum to the sum of the pure secondary structure Raman spectra (PSSRS). The Raman spectral regions between  $1420\text{--}1484\text{ cm}^{-1}$  and  $1572\text{--}1620\text{ cm}^{-1}$  are not included in the amide spectral modeling, because of uncertainties in the assignments of features in these regions. The Raman spectral residuals were calculated as the difference between the experimentally observed and calculated spectra. The maximum spectral residuals were 8–12% of the Raman band intensities. However, for BI and BIII examined at high DPC or TFE concentrations, the maximum spectral residual values increased to 15%, because of subtraction artifacts.

Chi et al. (1998) previously discussed the accuracy of their methodology for determining secondary structure composition and showed that the fractional abundance of  $\alpha$ -helix,  $\beta$ -sheet, and random coil determined by PSSRS UV Raman corresponds well to the fractional abundance determined by x-ray crystallography. For highly helical proteins (i.e., hemoglobin and myoglobin), the relative  $\alpha$ -helix content calculated by x-ray crystallography and UV Raman spectroscopy differs by less than 10%. For less  $\alpha$ -helical proteins such as ribonuclease A ( $\sim 20\%$   $\alpha$ -helix), the  $\alpha$ -helix content difference calculated between x-ray crystallography and UV Raman spectroscopy is 3%, giving a  $\sim 15\%$  relative error. For even less  $\alpha$ -helical proteins such as trypsin ( $\sim 8\%$   $\alpha$ -helix), calculations of  $\alpha$ -helical contents from x-ray crystallography and UV Raman spectroscopy differ by  $\sim 50\%$ . (For further details, see Chi et al. (1998).)

## RESULTS

### pH dependence of conformation

Fig. 1 *A* shows the pH dependence of the BI 206.5-nm excited Raman spectra. The bands centered at  $\sim 1250$ ,  $1387$ ,  $1557$ , and  $1659\text{ cm}^{-1}$  are derived from the amide III, the  $C_{\alpha}\text{-H}$  bending, the amide II, and the amide I vibrations, respectively (Song and Asher, 1989; Wang et al., 1991; Chi et al., 1998). The  $C_{\alpha}\text{-H}$  band intensity, the amide III band frequency and intensity, and the intensity ratio of the amide I to the amide II bands are especially sensitive to protein

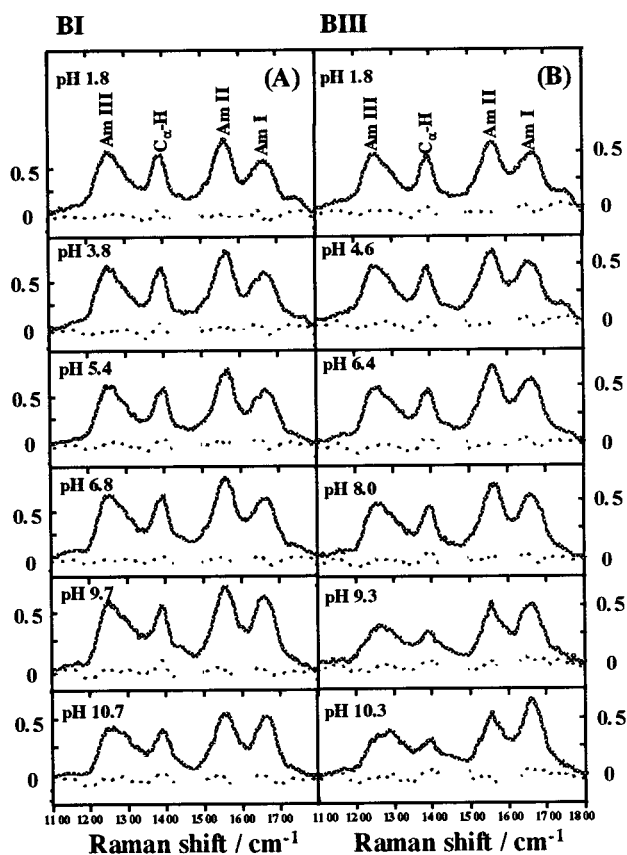


FIGURE 1 pH dependence of 206.5-nm excited Raman spectra and the calculated residuals of (A) BI and (B) BIII, respectively. Approximately 0.22 mM of BI and BIII was used in each measurement. The residuals were calculated as the difference between the experimentally obtained and calculated spectra. The Raman spectral regions between  $1420\text{--}1484\text{ cm}^{-1}$  and  $1572\text{--}1620\text{ cm}^{-1}$  are not included in the amide spectral modeling, because of the uncertainty of the spectral origin of contributions in these regions. Approximately 0.6 mW of 206.5-nm light is focused onto the sample with a spot size of  $\sim 80\text{ }\mu\text{m}$ . The spectra were collected on an ICCD detector with a total accumulation time of 5 min and a spectral resolution of  $\sim 20\text{ cm}^{-1}$ .

secondary structure (Holtz et al., 1996; Chi et al., 1998). The BI Raman spectrum at pH 1.8 shows a relatively intense  $C_{\alpha}\text{-H}$  bending band, which indicates that at pH 1.8, 0.22 mM BI is predominantly nonhelical (Wang et al., 1991; Holtz et al., 1996; Chi et al., 1998). Table 1, which lists the calculated pH dependence of the BI secondary structure content, indicates that BI remains predominately random coil and  $\beta$ -sheet between acid and neutral pH values (1%  $\alpha$ -helix, 42%  $\beta$ -sheet, and 57% random coil). These calculated secondary structural contents represent time-averaged values, and these results by themselves do not allow us to determine, for example, whether we have interconverting peptides of pure random coil and  $\beta$ -sheet content, or if each peptide simultaneously contains both random coil and  $\beta$ -sheet content.

As the pH increases from 6.8 to 10.7, the amide II and I bands modestly up-shift, whereas the amide I/amide II intensity ratio increases slightly. These spectral changes result

**TABLE 1** UV Raman determination of BI and BIII secondary structures as a function of pH

BI			BIII				
pH	$\alpha$ -Helix (%)	$\beta$ -sheet (%)	Random coil (%)	pH	$\alpha$ -Helix (%)	$\beta$ -sheet (%)	Random coil (%)
	1.8	0	37		63	1.8	2
3.8	0	42	58	4.6	13	40	47
5.4	0	43	57	6.4	22	34	44
6.8	1	42	57	8.0	25	36	39
8.4	10	39	51	9.3	48	31	21
9.7	24	35	41	10.3	60	19	21

from an increasing  $\alpha$ -helix content (at pH 10.7: 32%  $\alpha$ -helix, 31%  $\beta$ -sheet, and 37% random coil). This increased  $\alpha$ -helix content results from a loss mainly of random coil, but also from the loss of some  $\beta$ -sheet.

The pH dependence of the BIII conformation differs from that of BI (Figs. 1 B and 2). BIII is also nonhelical at pH 1.8 (2%  $\alpha$ -helix, 47%  $\beta$ -sheet, and 51% random coil). As the pH increases to pH 6.4, a large increase in  $\alpha$ -helical structure occurs; at pH 6.4, BIII consists of 22%  $\alpha$ -helix, 36%  $\beta$ -sheet, and 42% random coil (Table 1). Little additional secondary structural change occurs between pH 6.4 and pH 8. However, above pH 8, a further increase in  $\alpha$ -helix content occurs. Table 1 shows that at pH 10.3 the BIII secondary structure consists of 60%  $\alpha$ -helix, 19%  $\beta$ -sheet, and 21% random coil. The increase in the  $\alpha$ -helix content

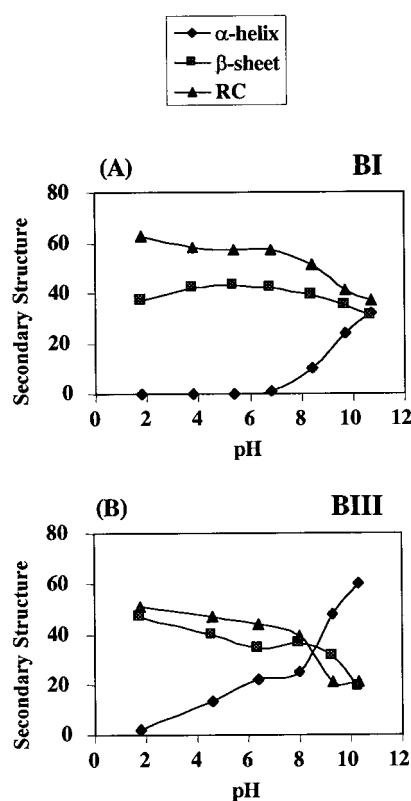


FIGURE 2 pH dependence of (A) BI and (B) BIII secondary structures.

results from similar decreases in  $\beta$ -sheet and random coil contents.

The different residues at positions 4–6 in BI and BIII are responsible for their different secondary structure titration behaviors between pH 1.8 and pH 8. An increased BIII  $\alpha$ -helical content at neutral pH occurs even though the  $\alpha$ -helical preferences of residues 4–6 are very similar to those of BI (Creighton, 1993). The lower pH BIII  $\alpha$ -helical formation titration midpoint occurs at pH  $\sim$ 4 (Fig. 2 B), which is close to the expected  $pK_a$  of 4.5 for Asp. This suggests that the increased BIII  $\alpha$ -helix content results from ion pairing between Lys<sub>2</sub> and Asp<sub>5</sub>. These ion pair species are separated by three residues;  $\alpha$ -helix stabilization by Glu<sup>-</sup>-Lys<sup>+</sup> ion pairs has previously been observed (Fairman et al., 1986). In fact, the observed neutral pH, 22%  $\alpha$ -helix content in BIII would correspond to one  $\alpha$ -helix turn, spanning the Lys<sub>2</sub> to Asp<sub>5</sub> sequence. The lack of this ion pair in BI results in the absence of  $\alpha$ -helix content.

The higher pH region of the titration curves shows midpoints around pH  $\sim$ 9.5, which correlates well with expected Lys  $pK_a$  values of 10. At neutral pH, repulsion between positively charged Lys residues in BI and BIII peptides

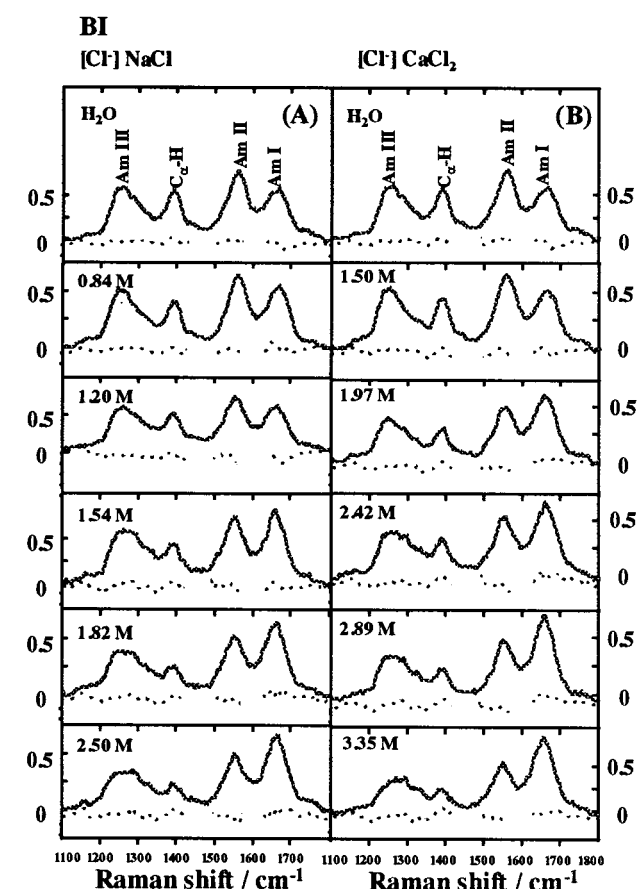


FIGURE 3 (A) NaCl and (B) CaCl<sub>2</sub> concentration dependence of BI 206.5-nm excited Raman spectra, and the calculated residuals. The secondary structural modeling and residual calculation parameters (laser power, spectral resolution, and the total accumulation time) are the same as in Fig. 1.

should oppose  $\alpha$ -helix formation. However, as these residues deprotonate at higher pH, additional  $\alpha$ -helical formation occurs. The His residue has a  $pK_a$  of  $\sim 6$  and does not appear to play a role in BI and BIII  $\alpha$ -helix formation. We conclude that at neutral pH, BIII has a single  $\alpha$ -helical turn localized close to the N-terminal region. Comparing the neutral pH secondary structural differences between BI and BIII, we conclude that the region spanning residues 4–6, which is  $\alpha$ -helical in BIII, is mainly random coil in BI. The similar decreases in the  $\beta$ -sheet and random coil contents of BIII as the pH increases from 2 to 8 indicate that at low pH residues 4–6 have  $\beta$ -sheet and random coil conformations (Fig. 2 B).

### Dependence of conformation on salts

Anion binding to proteins can induce conformational transitions (Goto et al., 1990; Goto and Hagihara, 1992). The

anion binding affinity for proteins follows the electroselectivity series of anions toward anion-exchange resins (Goto et al., 1990). Figs. 3, 4, and 5 show the UVRR spectral and the BI and BIII secondary structural dependence on increasing NaCl, CaCl<sub>2</sub>, NaClO<sub>4</sub>, and Ca(ClO<sub>4</sub>)<sub>2</sub> concentrations. ClO<sub>4</sub><sup>-</sup> is  $\sim 2.4$ -fold and  $\sim 10$ -fold more effective than Cl<sup>-</sup> in inducing  $\alpha$ -helix formation in BI and BIII, respectively. A similar stronger ClO<sub>4</sub><sup>-</sup> versus Cl<sup>-</sup> induction of  $\alpha$ -helix formation was also observed in melittin (Goto and Hagihara, 1992). Goto et al. (1990) proposed that the large impact of ClO<sub>4</sub><sup>-</sup> resulted from its smaller hydrodynamic radius, which made it easier for ClO<sub>4</sub><sup>-</sup> to ion pair with Lys residues.

The BIII  $\alpha$ -helix content increases at lower salt concentrations than does BI. For example, BIII saturates at  $\sim 70\%$   $\alpha$ -helix for  $\sim 0.15$  M NaClO<sub>4</sub> and Ca(ClO<sub>4</sub>)<sub>2</sub>, whereas BI requires a  $\sim 10$ -fold higher salt content. For the ClO<sub>4</sub><sup>-</sup> salts, there appears to be little difference between Na<sup>+</sup> and Ca<sup>2+</sup>. Significantly higher NaCl and CaCl<sub>2</sub> concentrations are

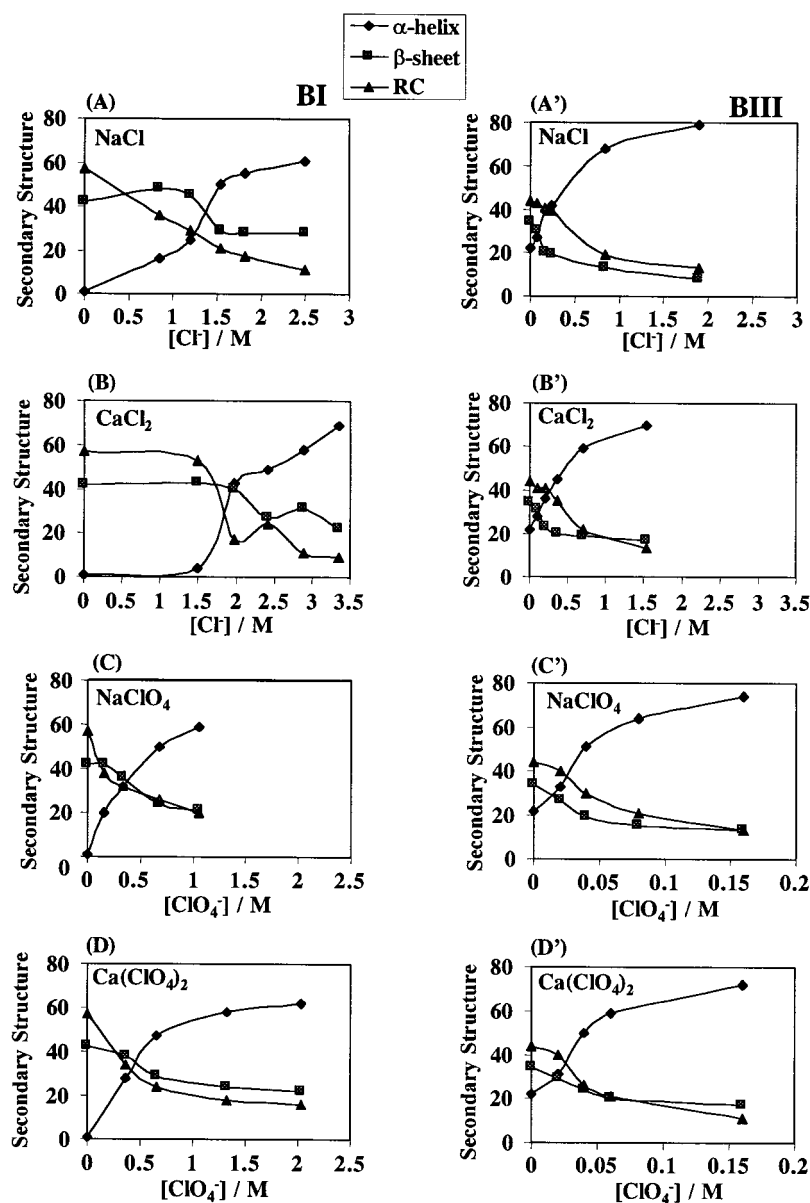


FIGURE 4 Anion concentration dependence of conformational transitions in (A, B, C, and D) BI and (A', B', C', and D') BIII, as examined using sodium and calcium salts of chloride and perchlorate.

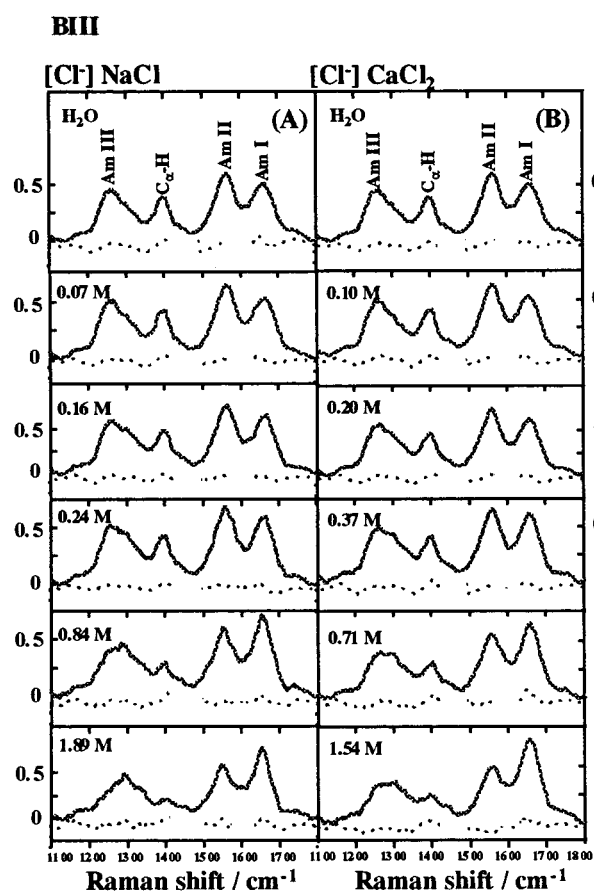


FIGURE 5 The 206.5-nm excited Raman spectra of BIII and their calculated residuals as a function of increasing (A) NaCl and (B) CaCl<sub>2</sub>, respectively. Secondary structural modeling, residual calculation, and experimental parameters are the same as in Fig. 1.

required to reach  $\sim 70\%$   $\alpha$ -helix for BIII and BI, but again BI is less  $\alpha$ -helical than BIII for a similar salt concentration. For BIII, Na<sup>+</sup> and Ca<sup>2+</sup> also act similarly. However, BI requires higher CaCl<sub>2</sub> than NaCl concentrations to give a similar  $\alpha$ -helix content.

### Dependence of conformation on trifluoroethanol

TFE stabilizes  $\alpha$ -helices by providing less polar solvating environments relative to H<sub>2</sub>O, which weakens water hydrogen bonding to peptides/proteins and favors compact peptide/protein structures that contain intramolecular hydrogen bonds (Cammers-Goodwin et al., 1996; Luo and Baldwin, 1997). Peptides with high helix propensity residues often reach their maximum helical content at  $\sim 30$ – $50\%$  TFE concentrations (Luo and Baldwin, 1997; Nelson and Kallenbach, 1989; Lehmann et al., 1990).

Figs. 6 and 7 demonstrate that increasing TFE concentrations increase the  $\alpha$ -helical contents of both BI and BIII. However, the existence of the initial BIII  $\alpha$ -helical turn at neutral pH results in an increased slope for the dependence of  $\alpha$ -helix content on TFE concentration. For BIII, the  $\alpha$ -helix content saturates at  $\sim 70\%$  by a  $\sim 15\%$  TFE con-

### TFE

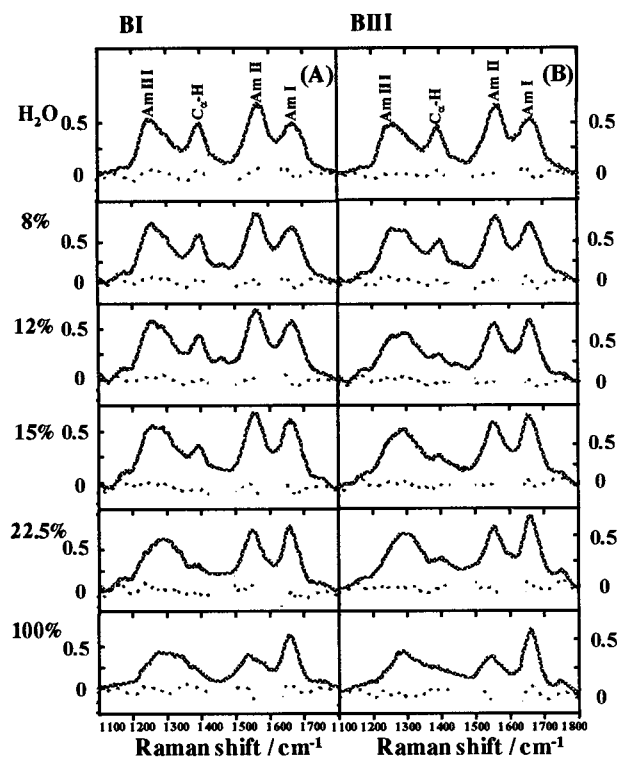


FIGURE 6 Excited Raman spectra (206.5 nm) and the calculated residuals of (A) BI and (B) BIII, respectively, in H<sub>2</sub>O and various TFE-H<sub>2</sub>O mixtures. Secondary structural modeling, residual calculation, and experimental parameters are the same as in Fig. 1.

centration, compared to the  $\sim 22.5\%$  TFE required for BI. TFE appears to convert BI and BIII to similar structures, because they both saturate at  $\sim 70\%$   $\alpha$ -helix and  $\sim 30\%$  random coil. It is likely that the middle regions of BI and BIII are  $\alpha$ -helical, whereas the approximately five penultimate terminal residues remain in random coil-type conformations.

### Dependence of conformation on DPC micelles

The  $\alpha$ -helix content of peptides often increases upon partitioning into micelles. The mechanism differs from that of TFE because the micellar interactions involve hydrophobic and/or amphiphilic environments, depending on the depth of peptide insertion into the micelles. The DPC lipid used here has a cmc of 1 mM and forms micelles with aggregation numbers of  $\sim 40$ . Fig. 8 shows the BI and BIII UVRr dependence on DPC concentration. An increase in the BI and BIII  $\alpha$ -helical content occurs even at DPC concentrations below the cmc (Fig. 9). For example, Fig. 9 illustrates that even at 1 mM DPC, BIII shows a significant increase in  $\alpha$ -helix content (from 22%  $\alpha$ -helix, 34%  $\beta$ -sheet, and 44% random coil to 47%  $\alpha$ -helix, 27%  $\beta$ -sheet, and 26% random coil). This indicates specific complexes between DPC and BI and BIII, such as nucleation of micelles around the peptides.

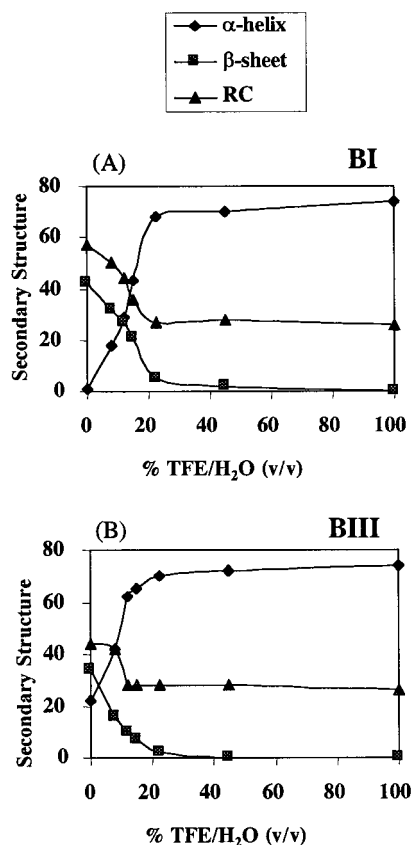


FIGURE 7 TFE concentration dependence of (A) BI and (B) BIII secondary structures, respectively.

At 1.78 mM DPC, BIII becomes predominately  $\alpha$ -helical (71%  $\alpha$ -helix). BI also shows an increased  $\alpha$ -helical content at 1.78 mM DPC (from 1% to 28%). At 3.6 mM DPC, the  $\alpha$ -helical contents of both BI and BIII almost saturate (65% and 71%  $\alpha$ -helix, respectively); DPC concentration increases above 3.6 mM further increase the BI and BIII  $\alpha$ -helix contents only modestly (Fig. 9). The presence of the initial BIII  $\alpha$ -helix turn is associated with its larger slope for the dependence of  $\alpha$ -helix content on DPC concentration than for BI.

### Self-association of BI and BIII

Amphiphilic  $\alpha$ -helices have high propensities for self-association. In very dilute aqueous solutions, amphiphilic peptides are monomeric and predominantly nonhelical (De-Grado et al., 1989). However, at higher peptide concentrations, alkaline pH, or high ionic strengths, many amphiphilic cytotoxic peptides become predominantly  $\alpha$ -helical and aggregated (Cornut et al., 1993). For example, melittin, an amphiphilic cytotoxin, aggregates into tetramers (Talbot et al., 1979; Bello et al., 1982; Quay and Condie, 1983; Dempsey, 1990; Goto and Hagihara, 1992; Wilcox and Eisenberg, 1992). This self-association process of amphiphilic  $\alpha$ -helices results from a subtle balance between two antagonistic effects: 1) a favorable hydrophobic effect

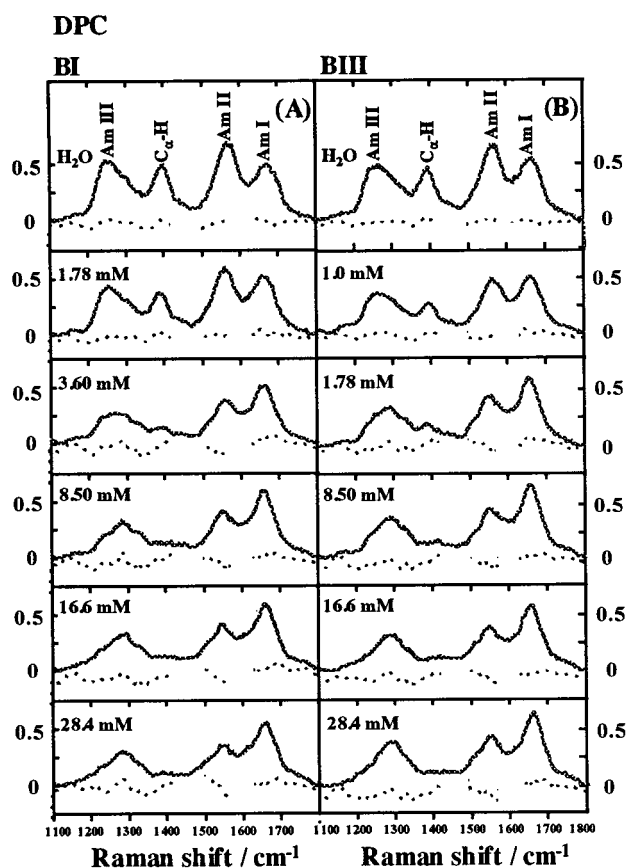


FIGURE 8 DPC concentration dependence of the 206.5-nm excited Raman spectra and the calculated residuals of (A) BI and (B) BIII, respectively. DPC critical micelle concentration is 1 mM. Secondary structural modeling, residual calculation, and experimental parameters are the same as in Fig. 1.

that draws the nonpolar faces of the amphiphilic  $\alpha$ -helices together, while exposing their polar faces to the surrounding aqueous environment; 2) a destabilizing formation of highly charged surfaces. Thus helix self-association is promoted by increasing peptide nonpolar domain sizes, and by minimizing charge repulsion between peptide monomers (Javadpour and Barkley, 1997; Cornut et al., 1993).

We used quasielastic light scattering to determine the aggregation state of BI and BIII in 0.2 M  $\text{Ca}(\text{ClO}_4)_2$ . BI and BIII solutions (0.22 mM) in pure water are essentially monomeric, because they show light scattering molecular masses of  $1.8 \times 10^3$  Da. In the presence of 0.2 M  $\text{Ca}(\text{ClO}_4)_2$ , we measure molecular masses of BI and BIII of  $5.8 \times 10^3$  and  $9.9 \times 10^3$  Da, respectively. Thus, in the presence of 0.2 M  $\text{Ca}(\text{ClO}_4)_2$ , the aggregation number for BI is  $\sim 3$ , whereas that for BIII is  $\sim 6$  (Table 2).

Our Raman results show that this aggregation is accompanied by an increased  $\alpha$ -helix content. This increased  $\alpha$ -helix formation with increasing salt concentration can result from either 1) a reduction in intramolecular electrostatic repulsion in BI and BIII that promotes  $\alpha$ -helix formation, which results in the self-association of hydrophobic faces of the amphiphilic helices, or 2) a self-association of

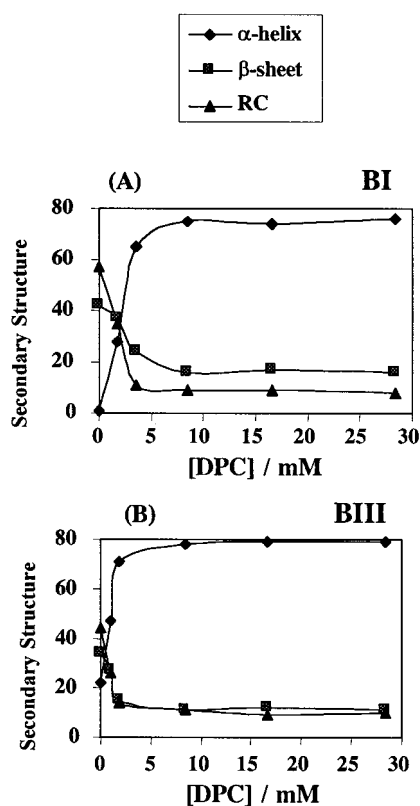


FIGURE 9 DPC concentration dependence of conformational transitions in (A) BI and (B) BIII.

the charge-screened, nonhelical peptides, which yields a more hydrophobic environment that promotes  $\alpha$ -helix formation. Unfortunately, we cannot distinguish between these two possibilities. BI is  $\sim 30\%$   $\alpha$ -helical at 0.2 M  $\text{Ca}(\text{ClO}_4)_2$ , whereas BIII is  $\sim 70\%$  helical (see Fig. 4, *D* and *D'*, respectively); at 0.2 M  $\text{Ca}(\text{ClO}_4)_2$ , BI aggregates into trimers, whereas BIII aggregates into hexamers. This is consistent with the observation of Bairaktari et al. (1990a,b) that BI aggregates less than BIII in similar solution conditions.

## DISCUSSION AND CONCLUSIONS

BI and BIII show essentially no  $\alpha$ -helical content at low pH and have somewhat more random coil than  $\beta$ -sheet content. Increasing the pH toward neutrality deprotonates the BIII  $\text{Asp}_5$ , which allows it to ion pair to  $\text{Lys}_2$ . No change occurs for BI until the pH is greater than 8. This BIII ion pair stabilizes a single  $\alpha$ -helical turn that causes a profound change in the environmental dependence of the BIII secondary structure compared to the identical peptide segments

TABLE 2 Molecular mass (Da) of BI and BIII in  $\text{H}_2\text{O}$  and 0.2 M  $\text{Ca}(\text{ClO}_4)_2$ , as determined by QELS

	$\text{H}_2\text{O}$	$\text{Ca}(\text{ClO}_4)_2$	Aggregation no.
BI	$1.8 \times 10^3$	$5.8 \times 10^3$	3.2
BIII	$1.8 \times 10^3$	$9.9 \times 10^3$	5.5

of BI. This  $\alpha$ -helical turn results in an increased  $\alpha$ -helical propensity in BIII over that of BI. Additional  $\alpha$ -helical structure is induced in BI and BIII by pH increases, which deprotonate Lys residues; the decrease in electrostatic repulsions promotes  $\alpha$ -helical conformations. A similar decrease in electrostatic repulsions and formation of  $\alpha$ -helical structure occurs upon the addition of anions such as  $\text{ClO}_4^-$ , which form ion pairs with protonated Lys residues.

The increased  $\alpha$ -helix propensity of BIII results from the fact that the most thermodynamically unfavorable step in  $\alpha$ -helix formation is the initial turn nucleation, because of the entropic cost for four residues to simultaneously assume an  $\alpha$ -helical turn (Creighton, 1993). After the first turn is formed, the addition of subsequent residues to the growing  $\alpha$ -helix requires only individual residues to assume correct orientations.

We can easily estimate the change in the Gibbs free energy,  $\Delta(\Delta G) = \Delta G_{\text{BIII}} - \Delta G_{\text{BI}}$  for  $\alpha$ -helix formation in BIII compared to BI. We utilize a model that assumes that the presence of  $\text{NaClO}_4$  induces an equilibrium between BI peptides of 100% versus zero  $\alpha$ -helical content, while it induces an equilibrium between BIII peptides of 100% versus 30%  $\alpha$ -helical content. This model presumes that the single  $\alpha$ -helical turn is locked in position and is not involved in the secondary structure equilibrium. For example, for the 0.05 M  $\text{NaClO}_4$  solution, we estimate a  $-1.2$  kcal/mol stabilization for formation of  $\alpha$ -helix in BIII compared to that in BI.

For BIII,  $\alpha$ -helix content increases will likely grow from the residues 4–6  $\alpha$ -helix loop at the N-terminal end, whereas for BI  $\alpha$ -helix nucleation may occur anywhere along the chain; however, the central role of Lys neutralization for  $\alpha$ -helix formation at high pH and at high salt suggests that the BI  $\alpha$ -helix probably nucleates within the Lys-rich C-terminal end.

The formation of  $\alpha$ -helical structures in the presence of salts and presumably at high pH values is correlated with the aggregation of BI and BIII. This aggregation occurs under conditions where repulsions between protonated Lys are absent because of deprotonation of the quaternary amines at high pH or upon formation of ion pairs with added anions. The fact that BI and BIII at high salt concentrations show similar maximum  $\alpha$ -helix contents and similar residual random coil and  $\beta$ -sheet contents suggests that the final structures for these peptides are similar at high salt. The conformations in TFE of BI and BIII also appear identical, but the conformations differ from that at high salt; at high TFE concentrations, BI and BIII saturate at 70%  $\alpha$ -helix and 30% random coil, without the  $\beta$ -sheet observed at high salt. In contrast, in DPC micelles we see identical BI and BIII conformations that resemble those at high salt. This may result from formation of ion pairs with DPC headgroups that promote  $\alpha$ -helix conformation.

*Note Added in Proof:* After completion of this manuscript, a paper on the aggregation and conformational transition in aqueous solution of a BIII

analog was published (Cabrele et al., 1997). Cabrele et al. photopolymerized a BIII analog into dimers and determined, using CD, that its  $\alpha$ -helix content is peptide concentration dependent. Cabrele et al. speculated that  $\alpha$ -helical formation in the BIII analog dimer is accompanied by aggregation of at least two BIII analog dimers. Our QELS results show directly that BIII molecules self-associate into hexamers at 0.2 M  $\text{Ca}(\text{ClO}_4)_2$ . Cabrele et al. also examined the conformational dependence of BIII and BIII analogs on KCl, with a fixed KCl concentration and increasing peptide concentrations. In the presence of KCl, Cabrele et al. found that the  $\alpha$ -helix formation occurs at lower BIII and BIII analog concentrations than in pure  $\text{H}_2\text{O}$ . This is expected because the salt screens the electrostatic repulsions within and/or between the peptides, thus promoting  $\alpha$ -helix formation.

We thank Dr. Michelle Chen from Wyatt Technology Corporation for providing the QELS results. We also thank Drs. Kasi V. Somayajula and Andrew A. Amoscato and Prof. Joe Grabowski for helpful discussions.

We gratefully acknowledge support from National Institutes of Health grant R01GM30741-16.

## REFERENCES

- Albert, J. S., and A. D. Hamilton. 1995. Stabilization of helical domains in short peptides using hydrophobic interactions. *Biochemistry*. 34: 984–990.
- Argiolas, A., and J. J. Pisano. 1985. Bombolitins, a new class of mast cell degranulating peptides from the venom of the bumblebee *Megabombus pennsylvanicus*. *J. Biol. Chem.* 260:1437–1444.
- Asher, S. A. 1993a. UV Raman spectroscopy for analytical, physical, and biophysical chemistry. *Anal. Chem.* 65:59A–66A.
- Asher, S. A. 1993b. UV Raman spectroscopy for analytical, physical, and biophysical chemistry. *Anal. Chem.* 65:201A–210A.
- Asher, S. A., C. R. Johnson, and J. Murtaugh. 1983. Development of a new UV resonance Raman spectrometer for the 217–400-nm spectral region. *Rev. Sci. Instrum.* 54:1657–1662.
- Bairaktari, E., D. F. Mierke, S. Mammi, and E. Peggion. 1990a. Conformations of bombolitins I and III in aqueous solutions: circular dichroism,  $^1\text{H}$  NMR, and computer simulations studies. *Biochemistry*. 29: 10097–10102.
- Bairaktari, E., D. F. Mierke, S. Mammi, and E. Peggion. 1990b. Conformational studies by circular dichroism,  $^1\text{H}$  NMR, and computer simulations of bombolitins I and III in aqueous solution containing surfactant micelles. *Biochemistry*. 29:10090–10096.
- Bello, J., H. R. Bello, and E. Granados. 1982. Conformation and aggregation of melittin: dependence on pH and concentration. *Biochemistry*. 21:461–465.
- Cabrele, C., S. Furin, M. Gurrath, S. Mammi, and E. Schievano, and E. Peggion. 1997. Aggregation and conformational transition in aqueous solution of a bombolitin III analogue containing a photoreactive side-chain group. *Biopolymers*. 42:147–156.
- Cammers-Goodwin, A., T. J. Allen, S. L. Oslick, K. F. McClure, J. H. Lee, and D. S. Kemp. 1996. Mechanisms of stabilization of helical conformations of polypeptides by water containing trifluoroethanol. *J. Am. Chem. Soc.* 118:3082–3090.
- Chi, Z., X. Chen, J. S. W. Holtz, and S. A. Asher. 1998. UV resonance Raman selective amide vibrational enhancement quantitative methodology for determining protein secondary structure. *Biochemistry*. 37: 2854–2864.
- Chupin, V., J. A. Killian, J. Breg, H. H. J. de Jongh, R. Boelens, R. Kaptein, and B. de Kruijff. 1995. PhoE signal peptide inserts into micelles as a dynamic helix-break-helix structure, which is modulated by the environment. A two-dimensional  $^1\text{H}$  NMR study. *Biochemistry*. 34:11617–11624.
- Cornutt, I., E. Thiaudiere, and J. Dufourcq. 1993. The amphipathic helix in cytotoxic peptides. In *The Amphipathic Helix*. R. M. Epand, editor. CRC Press, Boca Raton, FL. 173–219.
- Creighton, T. E. 1993. *Proteins—Structures and Molecular Properties*, 2nd Ed. W. H. Freeman and Company, New York.
- DeGrado, W. F., Z. R. Wasserman, and J. D. Lear. 1989. Protein design, a minimalist approach. *Science*. 243:622–628.
- Dempsey, C. E. 1990. The actions of melittin on membranes. *Biochim. Biophys. Acta.* 1031:143–161.
- Fairman, R., H. G. Cho, T. B. Lavoie, J. J. Villafranca, G. R. Matsueday, and J. Novotny. 1986. Design of heterotetrameric coiled coils: evidence for increased stabilization by  $\text{Glu}^- \text{Lys}^+$  ion pair interactions. *Biochemistry*. 35:2824–2829.
- Goto, Y., and Y. Hagihara. 1992. Mechanism of acid-induced folding of proteins. *Biochemistry*. 31:732–738.
- Goto, Y., N. Takahashi, and A. L. Fink. 1990. Mechanisms of acid-induced folding of proteins. *Biochemistry*. 29:3480–3488.
- Holtz, J. S. W., R. W. Bormett, Z. Chi, N. Cho, X. G. Chen, V. Pajcini, S. A. Asher, L. Spinelli, P. Owens, and M. Arrigoni. 1996. Applications of a new 206.5-nm continuous wave laser source: UV Raman determination of protein secondary structure and CVD diamond material properties. *Appl. Spectrosc.* 50:1459–1468.
- Javadpour, M. M., and M. D. Barkley. 1997. Self-assembly of designed antimicrobial peptides in solution and micelles. *Biochemistry*. 36: 9540–9549.
- Lehrmann, S. R., J. L. Tuls, and M. Lund. 1990. Peptide  $\alpha$ -helicity in aqueous trifluoroethanol: correlations with predicted  $\alpha$ -helicity and the secondary structure of the corresponding regions of bovine growth hormone. *Biochemistry*. 29:5590–5596.
- Luo, P., and R. L. Baldwin. 1997. Mechanism of helix induction by trifluoroethanol: a framework for extrapolating the helix-forming properties of peptides from trifluoroethanol/water mixtures back to water. *Biochemistry*. 36:8413–8421.
- Nelson, J. W., and N. R. Kallenbach. 1989. Stabilization of the ribonuclease s-peptide  $\alpha$ -helix by trifluoroethanol. *Biochemistry*. 28:5256–5261.
- Quay, S. C., and C. C. Condie. 1983. Conformational studies of aqueous melittin: thermodynamic parameters of the monomer-tetramer self-association reaction. *Biochemistry*. 22:695–700.
- Song, S., and S. A. Asher. 1989. UV resonance Raman studies of peptide conformation in poly(L-lysine), poly(L-glutamic acid), and model complexes: the basis for protein secondary structure determinations. *J. Am. Chem. Soc.* 111:4295–4305.
- Talbot, J. C., J. Dufourcq, J. de Bony, J. F. Faucon, and C. Lussan. 1979. Conformational change and self-association of monomeric melittin. *FEBS Lett.* 102:191–193.
- Wang, Y., R. Purrello, T. Jordan, and T. G. Spiro. 1991. UVRR spectroscopy of the peptide bond. I. Amide S, a nonhelical structure marker, is a  $\text{C}_\alpha\text{-H}$  bending mode. *J. Am. Chem. Soc.* 113:6359–6368.
- Waterhouse, D. V., and W. C. Johnson, Jr. 1994. Importance of environment in determining secondary structure in proteins. *Biochemistry*. 33: 2121–2128.
- Wilcox, W., and D. Eisenberg. 1992. Thermodynamics of melittin tetramerization determined by circular dichroism and implications for protein folding. *Protein Sci.* 1:641–653.